https://doi.org/10.5194/egusphere-2026-2078
Preprint. Discussion started: 20 May 2026

Relativistic runaway electron avalanches: unified density-dependent scaling and transport

Liza Hovhannisyan (hovhannisyanliza84@gmail.com)

A. I. Alikhanyan National Laboratory (Yerevan Physics Institute), Yerevan, Armenia

Abstract

Relativistic runaway electron avalanches (RREA) play a key role in producing high-energy radiation in thunderstorm environments, yet their quantitative description remains largely empirical, with limited validation across atmospheric conditions. In this work, we develop a unified framework that consistently describes both avalanche development within the electric field and particle propagation beyond it, using CORSIKA simulations at four high-altitude stations spanning a wide range of atmospheric densities. We show that the classical relation for avalanche length requires revision: the empirical coefficient K is not universal but varies systematically with atmospheric density. Introducing density-dependent scaling yields a consistent description of avalanche growth across all sites. At the same time, we identify an effective energy-partition coefficient, calibrated at a characteristic propagation scale of 100 m, which remains stable across all stations and reflects the available propagation after exiting a strong acceleration field. The results demonstrate that RREA can be described as a two-stage physical system that links density-dependent avalanche growth with density-dependent particle transport via a universal energy-partition mechanism. This framework provides a compact and physically transparent basis for interpreting high-energy atmospheric phenomena across altitudes.

1. Introduction

High-energy particle phenomena in the atmosphere constitute a rapidly developing field at the intersection of cosmic-ray physics, atmospheric electricity, and climatology. Over the past decades, a wide variety of particle bursts have been observed at the Earth's surface, in the atmosphere, and from space by satellite-borne spectrometers, including thunderstorm ground enhancements (TGEs), gamma-ray glows, and terrestrial gamma-ray flashes (TGFs) (Chilingarian et al., 2010; Fishman et al., 1994; Dwyer et al., 2012). Despite the diversity of detection platforms and energy ranges, mounting experimental evidence suggests that these phenomena are closely related and arise from electron acceleration in atmospheric electric fields (Dwyer and Uman, 2014). The physical origin of these bursts remains an active area of research. Although the microphysics of gamma-ray production, electron acceleration, and electromagnetic interactions in air are well established (Bethe and Heitler, 1934; Koch and Motz, 1959), the atmospheric environment in which these processes occur is highly

https://doi.org/10.5194/egusphere-2026-2078
Preprint. Discussion started: 20 May 2026

dynamic and difficult to characterize. In particular, the rapid temporal evolution and complex spatial structure of atmospheric electric fields within thunderclouds preclude a fully analytical treatment of particle acceleration. Consequently, much of the progress in this field has relied on empirical or semi-empirical formulations that capture the essential behavior of energetic particle populations without requiring detailed knowledge of the instantaneous electric-field configuration (Gurevich et al., 1992; Dwyer, 2003).

A key step in the theoretical description of particle acceleration under thunderstorm conditions was the development of the relativistic runaway electron avalanche (RREA, Gurevich et al., 1992; Dwyer, 2003). In sufficiently strong atmospheric electric fields (AEFs), energetic electrons can overcome ionization losses and enter a runaway regime, where they continue to gain energy from the electric field and produce secondary electrons through collisions with air molecules. This process leads to an avalanche multiplication of electrons and the accompanying production of high-energy bremsstrahlung gamma rays. A central parameter characterizing this avalanche development is the e-folding length λ (E, ρ), which describes the characteristic distance over which the number of runaway electrons grows exponentially. A widely used empirical description of this process was introduced by Dwyer (2003), who proposed the relation

$$\lambda(E,\rho) = \frac{K}{E_z - E_{\mathrm{th}}(h)}, \quad (1)$$

Where E_z and $E_{th}(h)$ (the runaway threshold electric field) are expressed in kV/m, λ is in meters, and K in kV. ρ_0 = 1.225 kg/m^3 is the air density at sea level, and ρ is the air density at altitude z. Empirical constant K is usually set to 7.2×10^3 kV. While this equation has been widely applied, it does not explicitly account for variations in AEF and atmospheric density and is often limited to narrow altitude and AEF ranges.

In parallel, the concept of free path distance (FPD) has been introduced as a phenomenological quantity that characterizes the ability of energetic particles to propagate beyond the electric-field region and reach ground-based detectors (Chilingarian et al., 2020; Chilingarian et al., 2022). Although this approach provides a useful link between simulations and observations, its empirical coefficients are constrained by limited datasets and simplified assumptions. The complex, highly variable structure of atmospheric electric fields makes a fully analytical treatment of these processes difficult. As a result, empirical formulations remain essential, but their reliability depends on systematic validation across a wide range of atmospheric conditions. In this context, modern Monte Carlo simulations offer a powerful tool for deriving physically consistent descriptions of particle acceleration and transport in realistic environments (Heck et al., 1998).

https://doi.org/10.5194/egusphere-2026-2078
Preprint. Discussion started: 20 May 2026

In this work, we revisit and optimize two key empirical relations that describe complementary stages of RREA evolution: avalanche development within the electric field and particle propagation beyond it. Both are derived from a unified CORSIKA-based simulation framework applied to multiple high-altitude stations with varying atmospheric densities. This approach directly links the internal dynamics of avalanche growth to subsequent particle transport. Unlike previous studies, which typically treat these processes independently, we establish a coherent set of empirical relations that consistently describe both particle multiplication and propagation within a single physical framework. All model parameters are derived directly from simulation data, without arbitrary assumptions. In particular, we identify a proportionality between electron and gamma-ray energies at the field boundary and explicitly account for density-dependent energy losses during propagation. The resulting formulation provides a physically transparent, quantitatively consistent description of high-energy particle transport in thunderstorm environments and offers a unified basis for interpreting observations at different altitudes.

2. Simulation Framework

To investigate the development of relativistic runaway electron avalanches (RREA) and the subsequent propagation of energetic particles under realistic atmospheric conditions, we performed Monte Carlo simulations using the CORSIKA (COsmic Ray SImulations for KAscade) code (Heck et al., 1998), version 7.7500, which includes the effect of atmospheric electric fields on particle transport (Buitink et al., 2009). The same simulation setup is used consistently throughout this work to describe both avalanche growth inside the electric field and particle propagation beyond it.

The atmospheric electric field was modeled as a vertically oriented uniform layer with a total thickness of 2000 m above the detector level. Although simplified, this configuration provides a widely used approximation of strong electric-field regions inside thunderclouds. To resolve the longitudinal development of particle populations, the field region was subdivided into 20 layers of 100 m each, and particle numbers were recorded at each boundary. This setup allows reconstruction of the depth-dependent evolution of electron and gamma-ray populations within the electric field.

In addition to the observation levels within the electric-field region, an additional level was defined at the lower boundary of the electric field *(exit)*, as well as a detector level *(det)* located 100 m below this boundary, corresponding to the station altitude above sea level. These levels enable the analysis of particle propagation beyond the electric-field region and provide the basis for the determination of the free path distance (FPD) described in the following sections.

Simulations were performed for four high-altitude observational stations with distinct atmospheric densities: Aragats (ρ = 0.77 kg/m³, roughly 3000 m above sea level), Nor Amberd (ρ = 0.89 kg/m³, about 2000 m above sea level), Lomnický Štít (ρ = 0.83 kg/m³, approximately 2600 m above sea level), and LHAASO (ρ = 0.66 kg/m³, around 4400 m above sea level). In the simulation setup, the

https://doi.org/10.5194/egusphere-2026-2078
Preprint. Discussion started: 20 May 2026

electric-field layer begins 2 km above each station, at altitudes ranging from 4000 m to 6400 m, providing a suitable atmospheric density range for studying how avalanche development depends on altitude. The electric field strengths used in the simulations ranged from 180 to 260 kV/m, depending on the altitude of the observational site. These values were selected so that the applied electric field exceeds the runaway threshold field $E_{th}(h)$ by a sufficient margin to ensure the exponential growth of the electron population characteristic of relativistic runaway electron avalanches. The runaway threshold electric field is defined as $E_{th}(h) = E_0 \cdot n(h)$, where E_0 is the threshold field at sea level and $n(h) = \rho(h)/\rho_0$ is the normalized atmospheric density. In this work, we adopt E_0 = 284 kV/m, consistent with previous studies. In particular, the chosen field strengths satisfy the condition $E_z - E_{th}(h) > 0$ with a significant excess above the threshold, allowing the avalanche process to develop over the entire electric-field region. At the same time, the selected range corresponds to physically realistic thunderstorm conditions, where electric fields are sufficiently strong to support RREA development but remain below levels that would rapidly trigger lightning discharges. Each simulation corresponds to the injection of a single seed electron into the electric-field region. The initial energy spectrum was adopted from the EXPACS model (Sato, 2016) and follows a power-law distribution with an index of 1.173 in the energy range 1–300 MeV. To ensure statistical stability, 500–1000 simulation events were performed for each field configuration.

During particle propagation, electrons and gamma rays were tracked until their energies decreased to 0.05 MeV. At each observation level within the electric-field region, the numbers of electrons and gamma rays were recorded. In the analysis presented below, particular attention is given to the electron population $N_e(d)$, *which* is used to determine the effective avalanche length, while the comparison of particle spectra at the field boundary and below it provides the basis for the FPD analysis. This simulation framework provides the basis for quantifying avalanche development, which is analyzed in the following section.

3. Avalanche Development within the AEF

The longitudinal profiles of the electron population from CORSIKA simulations provide a basis for determining the effective avalanche length of relativistic runaway electron avalanches. As described in the previous section, particle numbers were recorded at regular depth intervals of 100 m within the electric-field layer of thickness L=2000 m above the station. To minimize boundary effects, heights within 100 m from the observation level were excluded from the fitting process. For each value of the applied electric field and each observational site, the simulations produce a depth-dependent electron population, $N_e(d)$, where d denotes the downward propagation distance from the top of the electric-field layer. The absolute height H is then given by:

$$H = H_{st} + 2000 - d$$

https://doi.org/10.5194/egusphere-2026-2078
Preprint. Discussion started: 20 May 2026

When the electric field exceeds the runaway threshold field $E_{th}(h)$, the number of runaway electrons increases approximately exponentially with propagation distance. In this regime, the development of the avalanche can be described by the relation

$$N_e(d)=N_0e^{d/\lambda},$$

where N_0 is the number of initial seed electrons, and λ is the characteristic avalanche length. According to Eq. (1), this parameter represents the distance over which the number of runaway electrons increases by a factor of e.

Taking the natural logarithm of the expression above yields a linear dependence of the form

$$lnN_e(d)=c+bd,$$

where $c=lnN_0$ and $b=1/\lambda$. Thus, the avalanche length can be obtained from the slope of the linear fit to the logarithmic electron profile.

For each simulated electric field strength the depth dependence of the electron population $N_e(d)$ was first averaged over the ensemble of simulation events in order to obtain statistically stable profiles. The natural logarithm of the averaged electron counts was then fitted as a function of depth using a linear regression. The resulting slope parameter b provides a direct estimate of the effective avalanche length,

$$\lambda_{eff} = 1/b.$$

Repeating this process for various electric-field strengths and across all observational sites produces a set of effective avalanche lengths, λ_{eff}, corresponding to different values of the electric-field excess, $E_z - E_{th}(h)$. These values serve as the basis for optimizing the empirical coefficient K in the avalanche-length relation (Eq. (1)). To evaluate the validity of the classical scaling relation, we now compare the extracted avalanche lengths with the expected dependence on the electric-field excess.

The coefficient $K \approx 7.2\times10^3$ kV, widely used in the literature (Dwyer, 2003), was originally derived for a limited set of atmospheric conditions and has not been systematically validated across a broad range of altitudes. Despite this limitation, it has been extensively adopted in analytical descriptions of avalanche growth and in phenomenological models of particle acceleration in atmospheric electric fields, motivating a reassessment of its universality.

The universality of the coefficient K at various heights and AEFs remains an unresolved issue. The original estimate was derived for a very high AEF of 300 kV/m; our Monte Carlo simulations enable the study of RREA development across a wider range of electric-field strengths and atmospheric densities. Specifically, simulations at different altitudes provide an opportunity to determine whether a single universal value of K can effectively represent avalanche development in environments with significantly different heights and air densities.

https://doi.org/10.5194/egusphere-2026-2078
Preprint. Discussion started: 20 May 2026

For each simulated electric-field value and for each observational site, the variable

$$x=1/(E_z - E_{th}(h)),$$

was computed. According to the classical formulation of the avalanche-length relation, the avalanche length should depend linearly on this variable:

$$\lambda=Kx.$$

Thus, the coefficient K can be determined by fitting a straight line through the origin in the (x, λ_{eff}) parameter space.

The fitting procedure was performed using the least-squares method constrained to pass through the origin. In this case, the optimal value of the coefficient is given by

$$K=\sum_i \lambda_i x_i / \sum_i x_i^2 ,$$

where x_i and λ_i correspond to the values obtained for different electric-field strengths within each station.

Applying this procedure to the CORSIKA simulation results yields station-specific estimates of the empirical coefficient. The resulting coefficients are:

$$K_{Aragats} \approx 10.2 \times 10^3 kV.$$

$$K_{LHAASO} \approx 11.2 \times 10^3 kV.$$

$$K_{Lomnicky'} \approx 8.97 \times 10^3 kV,$$

$$K_{NorAmberd} \approx 8.58 \times 10^3 kV.$$

The observed deviations from the classical scaling suggest that additional physical factors must be taken into account. These results demonstrate that the empirical coefficient derived from CORSIKA simulations is systematically larger than the classical value $K=7.2\times10^3\ kV$ proposed by Dwyer. At the same time, the optimized coefficients show noticeable variation between stations, spanning the interval

$$K \sim 8.58 \times 10^3 - 11.2 \times 10^3 kV.$$

Such variability suggests that the assumption of a universal constant K may not fully account for the way avalanche development depends on atmospheric conditions. Specifically, stations at different altitudes experience significantly different air densities, which influence both the runaway threshold field and the efficiency of avalanche multiplication.

For reference, the average value obtained from the four stations located at 2000 - 4400 m (AEF introduce 2000 m higher) is approximately

$$K_{global} \approx 9.58 \times 10^3 kV.$$

https://doi.org/10.5194/egusphere-2026-2078
Preprint. Discussion started: 20 May 2026

The station-dependent values of the empirical coefficient obtained in the previous section indicate that the classical avalanche-length scaling does not fully capture the physics governing the development of relativistic runaway electron avalanches in the atmosphere. The results obtained from the CORSIKA simulations reveal systematic deviations that depend on the observational site.

The stations considered in this work span a significant range of atmospheric densities, from approximately 0.66 kg/m^3 at the LHAASO observatory to about 0.89 kg/m^3 at Nor Amberd. Such differences correspond to substantial variations in the interaction environment experienced by runaway electrons. Although the threshold field $E_{th}(h)$ accounts for part of this dependence, it does not fully eliminate the influence of density on the avalanche multiplication rate.

These considerations motivate the introduction of an extended empirical scaling that explicitly includes a density-dependent factor in the avalanche length. This formulation allows the density dependence of avalanche development to be addressed directly rather than implicitly through changes in the empirical coefficient. To explicitly include this effect, we propose a generalized empirical formula where the avalanche length depends not only on the electric-field excess but also on the normalized atmospheric density. The revised relation is expressed as

$$\lambda(E,h)=K\, n(h)^a / (E_z - E_{th}(h)) \quad (2)\,,$$

where $n(h) = \rho(h)/\rho_o$ is the normalized air density, $\rho(h)$ is the local atmospheric density at altitude h, ρ_o = 1.225 kg/m³ is the air density at sea level, and a is an additional empirical exponent that explicitly describes the density dependence of avalanche development.

To determine the parameters of the relation (2), the effective avalanche lengths obtained from the CORSIKA simulations were fitted using the generalized scaling law. The fitting procedure simultaneously optimized the empirical coefficient K and the density exponent a by minimizing the deviations between simulated avalanche lengths and the extended model's predictions.

The best agreement is obtained from a joint optimization performed across all four stations, yielding

$$K \approx 6.39\times10^{3}\,kV,\ a \approx -0.92.$$

The negative exponent simply indicates that the avalanche length increases as the atmospheric density decreases. The introduction of the density-dependent term significantly improves the consistency of the scaling relation across stations located at different altitudes. In particular, when the modified scaling term $\lambda/n(h)^a$ is plotted as a function of the variable $1/(E_z - E_{th}(h))$, the simulation data from all stations collapse onto a single approximately linear relation, see Fig. 1. It summarizes the simulation results obtained for the four observational sites considered in this work and illustrates the ability of the models (1) and (2) to describe the dependence of the effective avalanche length on the electric-field strength.

https://doi.org/10.5194/egusphere-2026-2078
Preprint. Discussion started: 20 May 2026

Panel (a) displays the classical scaling of the effective avalanche length λ_{eff} as a function of $1/(E_z - E_{th}(h))$. The simulation results from different stations show an approximately linear trend; however, a clear scatter between stations is evident. Data points for various atmospheric densities do not perfectly align along a single line, indicating that the classical scaling does not fully account for the physical variability of avalanche development under different atmospheric conditions.

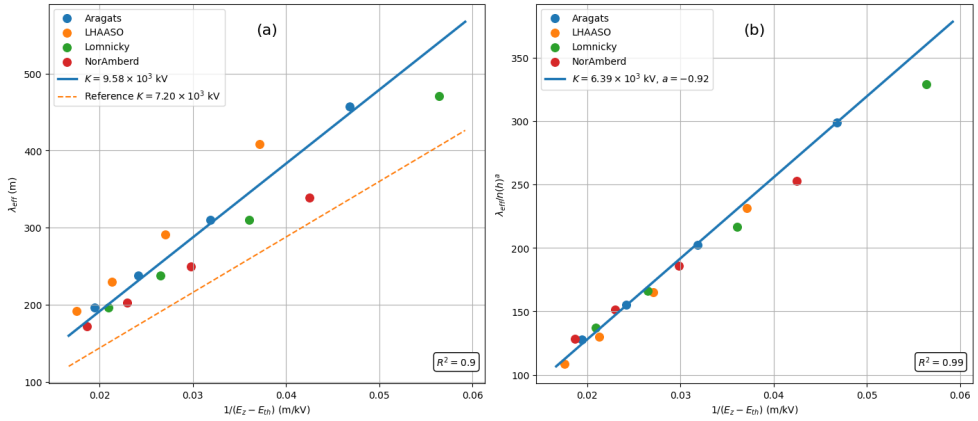

Figure 1. *Comparison of the classical and density-dependent scaling relations for the RREA avalanche length.*

Panel (b) uses the same simulation results after applying the density-dependent normalization introduced in the extended scaling relation. In this representation, the avalanche length is divided by the factor $n(h)^a$, where $n(h)=\rho(h)/\rho_0$ is the normalized atmospheric density and a is the empirical density exponent determined from the fitting procedure. Using the optimized parameters $K \approx 6.39 \times 10^3$ kV and $a \approx -0.92$, the simulation results from all stations collapse onto a single approximately linear relation.

To quantify the improvement of the density-dependent scaling over the classical formulation, the fitted coefficients and their corresponding coefficients of determination are summarized in Table 1. The effective coefficient $K_{eff}(h)$ is calculated from the extended scaling relation as $Kn(h)^a$, using the global fit parameters. As shown in the table, the modified Eq. (2) significantly outperforms the initial Eq. (1).

Table 1. *Comparison of the classical and density-dependent scaling relations for the RREA avalanche length. The coefficient of determination R^2 is shown for both models.*

Station	**$K_{classical}$(kV)**	**$K_{eff}(h) = K \cdot n(h)^a$(kV)**	**$R^2_{classical}$**	**$R^2_{extended}$**
Aragats	10.2×10^3	9.84×10^3	0.90	0.99

https://doi.org/10.5194/egusphere-2026-2078
Preprint. Discussion started: 20 May 2026

Station	**$K_{classical}$(kV)**	**$K_{eff}(h) = K \cdot n(h)^a$(kV)**	**$R^2_{classical}$**	**$R^2_{extended}$**
LHAASO	11.2×10^3	11.4×10^3	0.90	0.99
Lomnický Štít	8.97×10^3	9.20×103	0.90	0.99
Nor Amberd	8.58×10^3	8.53×10^3	0.90	0.99
Global fit	**9.58×10^3**	**6.39×10^3 (a= − 0.92)**	**0.90**	**0.99**

The quality of the linear correlation improves substantially, with the coefficient of determination increasing from $R^2 \approx 0.90$ in the classical scaling to $R^2 \approx 0.99$ in the extended formulation.

By explicitly incorporating this dependence, the extended empirical relation yields a unified scaling law that describes avalanche development across a broad range of altitudes and atmospheric conditions.

To better demonstrate the predictive performance of the modified estimate, a parity comparison between the simulated avalanche lengths and the values predicted by the models is presented in Fig. 2. In this representation, the horizontal axis corresponds to the effective avalanche length obtained from the CORSIKA simulations, while the vertical axis shows the values predicted by the empirical scaling relations. The diagonal line represents perfect agreement between predicted and simulated avalanche lengths. Points exactly on this line would represent an ideal model that perfectly reproduces the simulation results without systematic deviations.

As seen in Fig. 2, the classical scaling model exhibits noticeable deviations from the 1:1 relation, particularly for larger avalanche lengths. In contrast, the extended density-dependent formulation produces predictions that remain consistently closer to the ideal relation across the full range of simulated values. The improvement is reflected in the coefficient of determination, which increases from $R^2 \approx 0.90$ for the classical model to $R^2 \approx 0.99$ for the extended scaling.

https://doi.org/10.5194/egusphere-2026-2078
Preprint. Discussion started: 20 May 2026

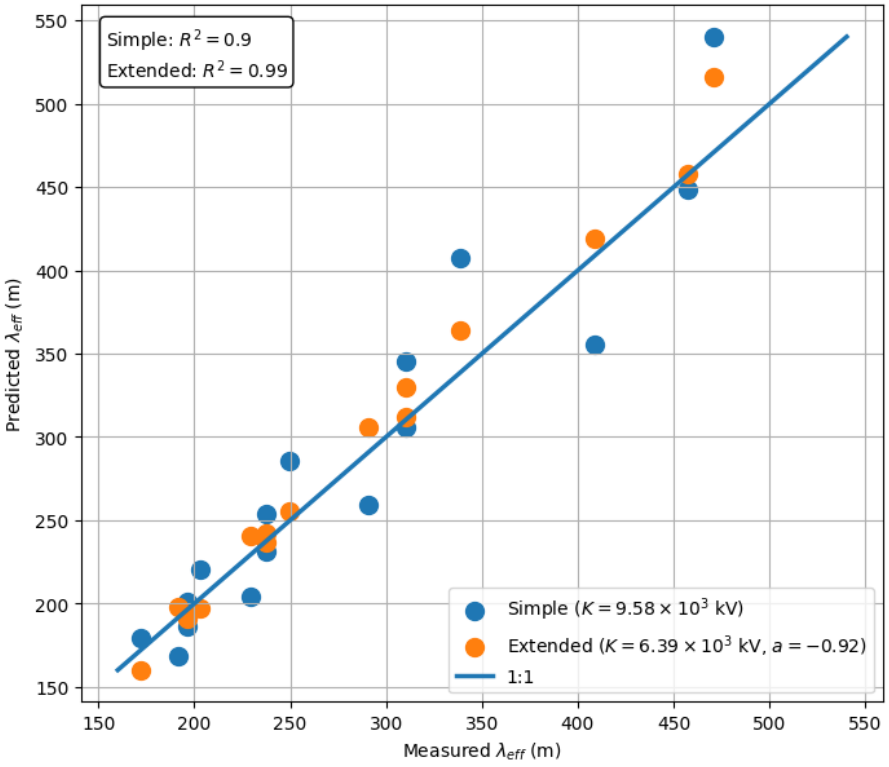

Figure 2. *Parity comparison between the effective avalanche lengths obtained from the CORSIKA simulations and the values predicted by the empirical scaling relations.*

In the next section, we will describe the avalanche propagation after departing from the strong acceleration AEF. Having established the scaling of avalanche growth within the electric field, we now turn to the propagation of particles beyond the field region.

4. Particle Propagation beyond the AEF

The key to recovering RREA energy spectra is understanding where the electric field above the spectrometer has dropped below the RREA threshold. When this gap is less than 100 m, a significant number of electrons will survive, enabling energy spectra and maximum energy recovery. If the maximum energy of electrons upon exiting the electric field and observed by the spectrometer is known, the approximate gap length (free path distance) can be estimated as:

$$FPD = \frac{E_e^{max}(exit) - E_e^{max}(det)}{C_2(h)},$$

https://doi.org/10.5194/egusphere-2026-2078
Preprint. Discussion started: 20 May 2026

where $C_2(h)$ is the well-known mean energy loss of the electron at altitude h. However, we do not know the maximum energy of electrons exiting the field region. Instead, we know the maximum energy of gamma rays reaching the spectrometer. Unlike electrons, which lose approximately constant ionization losses each cm, gamma rays can traverse the entire gap without producing electron-positron pairs and maintain the same maximum energy as at exit from the strong AEF. To quantitatively describe particle propagation beyond the accelerating electric-field region, an empirical equation for estimating the free path distance (FPD) was proposed by Chilingarian et al. (2020). Because the maximum electron energy at the field exit cannot be determined directly, we approximate it using the relation $E_e^{max}(exit) \approx C_1 \cdot E_\gamma^{max}(exit)$, which characterizes the energy partition between electrons and gamma rays in the avalanche. Substituting this relation into Eq. (3), we obtain the expression used in this work.

$$FPD = \frac{C_1 E_\gamma^{max}(exit) - E_e^{max}(det)}{C_2(h)} \quad (3)$$

Here $E_\gamma^{max}(exit)$ represents the characteristic gamma-ray energy at the exit of the electric-field region, $E_e^{max}(det)$ is the characteristic electron energy at the detector level, C_1 is an empirical coefficient reflecting the energy partition between gamma rays and electrons within the avalanche, and $C_2(h)$ is the altitude - dependent electron energy loss rate in air. The characteristic energies are defined using the characteristic maximum energy determined from the spectral distributions, based on the criterion of three consecutive energy bins with counts exceeding five events. We perform optimization studies to find a C_1 coefficient suitable for all stations discussed earlier. In simulations, the vertical gap between the RREA stopping height and the detector height is consistently set at 100 meters for all four stations. The electric field strengths were selected for each station as follows: Aragats (210 kV/m), LHAASO (190 kV/m), Lomnický Štít (220 kV/m), and Nor Amberd (240 kV/m). These values represent threshold supercritical regimes, avoiding both subcritical conditions, where avalanche multiplication is suppressed, and strongly supercritical fields, where nonlinear effects could distort the natural avalanche behavior. For each station, energy spectra of gamma rays and electrons were built at both the exit and detector levels. In the high-energy part of the spectra, where statistical fluctuations become important, a characteristic maximum energy E^{max} was defined using a reliable criterion: E^{max} is the highest energy at which at least three consecutive energy bins contain more than 5 counts. This definition reduces artificial spectrum extensions caused by outlier high-energy events and ensures that the identified endpoint reflects a stable physical feature of the distribution.

The spectral comparison between the exit and detector levels reveals two distinct propagation regimes for gamma rays and electrons. Gamma-ray spectra remain nearly constant over the 100 m propagation distance, with typical characteristic energies of $E_\gamma(exit) \approx$ 29–30 MeV and $E_\gamma(det) \approx$ 30–31 MeV. Thus, as expected, the maximum energy of gamma rays did not change over the 100 m path and can be used to estimate the electron's maximum energy at the entrance. A slight increase in the maximum gamma-

https://doi.org/10.5194/egusphere-2026-2078
Preprint. Discussion started: 20 May 2026

ray energy indicates additional bremsstrahlung production by electrons, whose exit energies are higher than those of the gamma rays. Conversely, electron spectra show a clear shift toward lower energies. At Aragats, the electron maximum energy dropped from approximately 38 MeV at exit to around 16 MeV at the detector after 100 m. Therefore, at exit, electrons possess higher energies than gamma rays, and before reaching the detector, electrons emit bremsstrahlung gamma rays with energies slightly higher than those in the electric field. This observation, shown in Fig. 3 and Fig. 4, provides a direct physical basis for relating the characteristic energies of electrons and gamma rays at the boundary of the electric field.

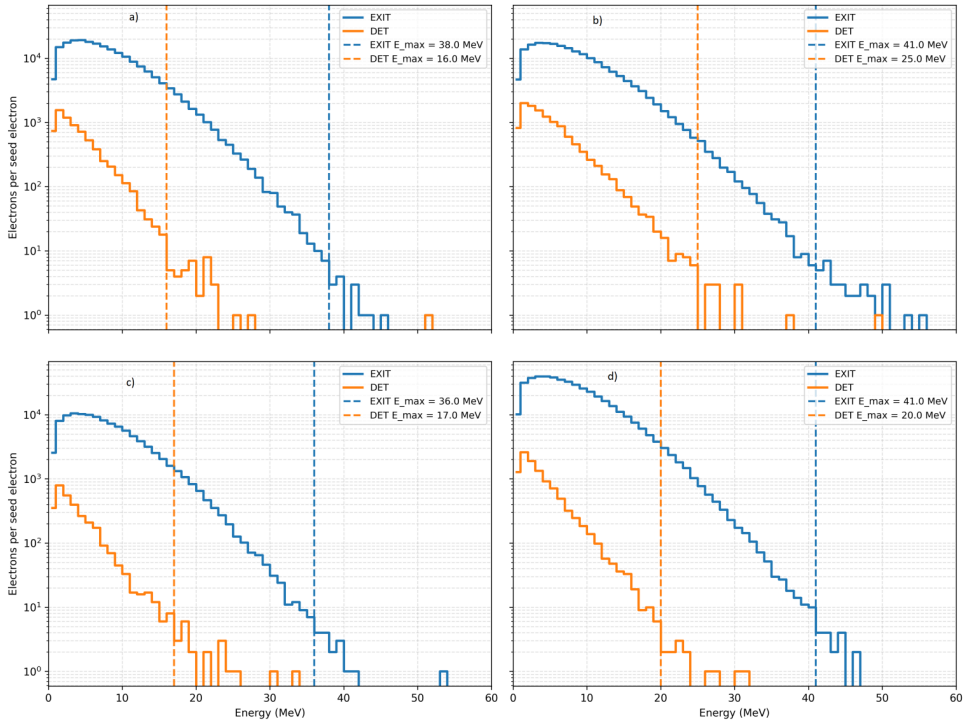

Figure 3. *The energy spectra of electrons at the exit and detector levels for all four stations: (a) Aragats (210 kV/m), (b) LHAASO (190 kV/m), (c) Lomnický Štít (220 kV/m), and (d) Nor Amberd (240 kV/m). The vertical separation between exit and detector is fixed at 100 m in all cases.*

https://doi.org/10.5194/egusphere-2026-2078
Preprint. Discussion started: 20 May 2026

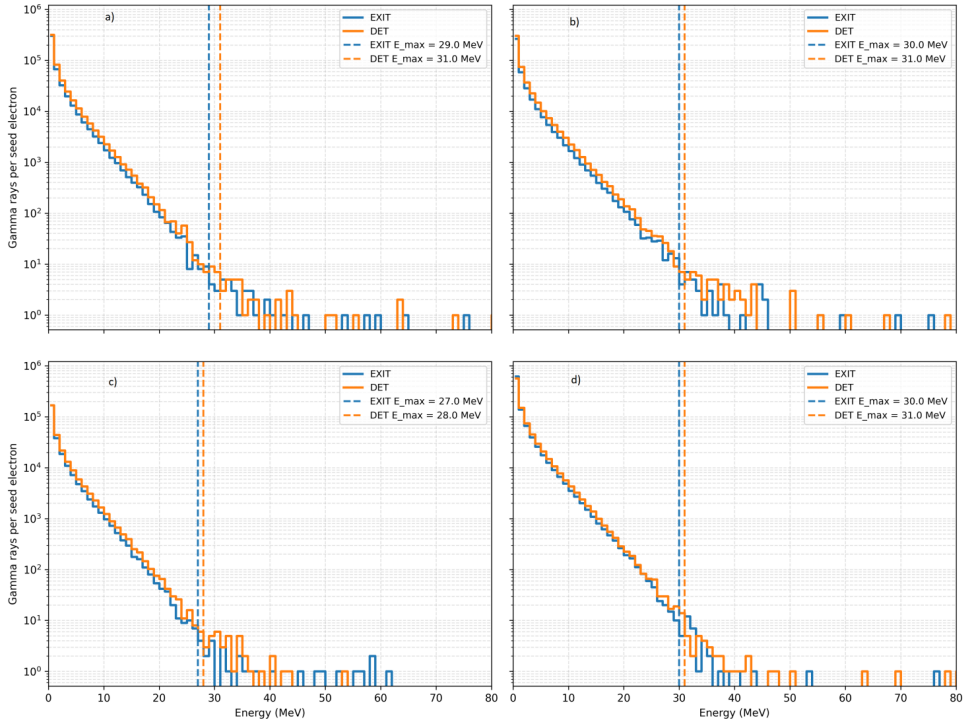

Figure 4*. The gamma-ray energy spectra at the exit and detector levels for the same four stations are shown. Unlike electrons, the high-energy cutoff remains nearly unchanged between the two levels, indicating that the maximum energy passing through 100 m at heights from 4000 to 6400 m remains constant. The effective maximum energies are indicated in the figure by vertical dashed lines.*

Thus, the simulation justifies using the maximum energy of gamma rays as a proxy for the electron maximum energy, with appropriate correction using the C_1 coefficient, see Eq. (3). The proportionality coefficient C_1 is derived directly from the exit and detector spectra using a bootstrap-based statistical procedure. For each station, the exit energy histograms of gamma rays and electrons were taken as the starting point. A Poisson bootstrap procedure was then applied, in which each energy bin count N_i was resampled according to

$$N_i^{(b)}(E) \sim Poisson(N_i),$$

where b denotes the bootstrap realization. In each bootstrap realization, every exit bin was resampled independently from a Poisson distribution with mean equal to the observed bin content. We use B = 2000 bootstrap realizations. The characteristic maximum energies $E_e(exit)^{(b)}$ and $E_\gamma(exit)^{(b)}$ were recalculated using the same three-consecutive-bins criterion. If $N(E_i)$ is the content of the i-th bin, we define i^* as the largest index for which $N(E_i)$, $N(E_{i-1})$, and $N(E_{i-2})$ all exceed 5 counts, and then set $E_\gamma(exit) = E_{i^*}$. Thus, the endpoint is a stable characteristic cutoff rather than the last isolated occupied

https://doi.org/10.5194/egusphere-2026-2078
Preprint. Discussion started: 20 May 2026

bin. The same procedure was used to estimate the effective maximum energy of electrons at detector height. Then, the corresponding coefficient was calculated as

$$C_1^{(b)} = (100 \cdot C_2(h) + E_e^{(b)}(det)) / E_\gamma^{(b)}(exit).$$

This definition ensures consistency between the coefficient and the physical model of particle propagation. Repeating this procedure over many bootstrap realizations yields for each station a distribution of C_1 values.

The median values obtained for individual stations are:

Aragats: $C_1 \approx 1.31$,

LHAASO: $C_1 \approx 1.39$,

Lomnický Štít: $C_1 \approx 1.46$,

Nor Amberd: $C_1 \approx 1.44$.

It should be noted that the coefficient C_1 reflects the energy partition between electrons and gamma rays within the avalanche, but in the present formulation it is calibrated using a characteristic propagation distance of 100 m. Therefore, it should be interpreted as an effective parameter linking avalanche dynamics at the field boundary with subsequent particle transport, rather than a purely intrinsic quantity. Its apparent stability across stations indicates a robust scaling of energy partition within the avalanche. The spread of the distributions is typically within ±0.03–0.05. Combining all bootstrap realizations from the four stations yields a global distribution with a pooled median of $C_1 \approx 1.38$. A global least-squares optimization, minimizing deviations of the predicted FPD from the expected 100 m scale, gives $C_1 \approx 1.375$. In the following, we adopt $C_1 \approx 1.37$ as the representative global coefficient.

The second parameter of the model, $C_2(h)$, characterizes the average energy loss of electrons per unit path length, which depends explicitly on atmospheric density. For each station, a representative energy for calculation losses was defined as

$$E^* = (E_e(exit) + E_e(det)) / 2,$$

which approximates the typical electron energy during propagation. The corresponding mass stopping power was obtained from the NIST ESTAR database using linear interpolation and multiplied by the local air density to obtain the linear stopping power.

The resulting values are

Aragats: $C_2 \approx 0.20$MeV/m,

LHAASO: $C_2 \approx 0.17$MeV/m,

Lomnicky Štít: $C_2 \approx 0.21$MeV/m,

Nor Amberd: $C_2 \approx 0.23$MeV/m.

https://doi.org/10.5194/egusphere-2026-2078
Preprint. Discussion started: 20 May 2026

The free path distance is then calculated according to Eq. (3), where $C_1$was derived from spectral data, $C_2(h)$ from stopping-power tables, and the energies from the simulated spectra.

Applying this expression to the simulation data for four stations yields FPD values ranging from 85 to 105 m., in agreement with the expected ~100 m scale.

To validate the optimized value of the proportionality coefficient C_1, we compare the resulting free path distance (FPD) values obtained using both the empirical coefficient (C_1 = 1.2) and the optimized coefficient ($C_1 \approx 1.37$). The FPD is computed for each bootstrap realization across all four stations using Eq. (3), preserving the full statistical variability of the simulated spectra.

The distributions of FPD values for each station are summarized in Fig. 5, where individual realizations are represented as density distributions, and the mean values with corresponding 68% intervals are indicated.

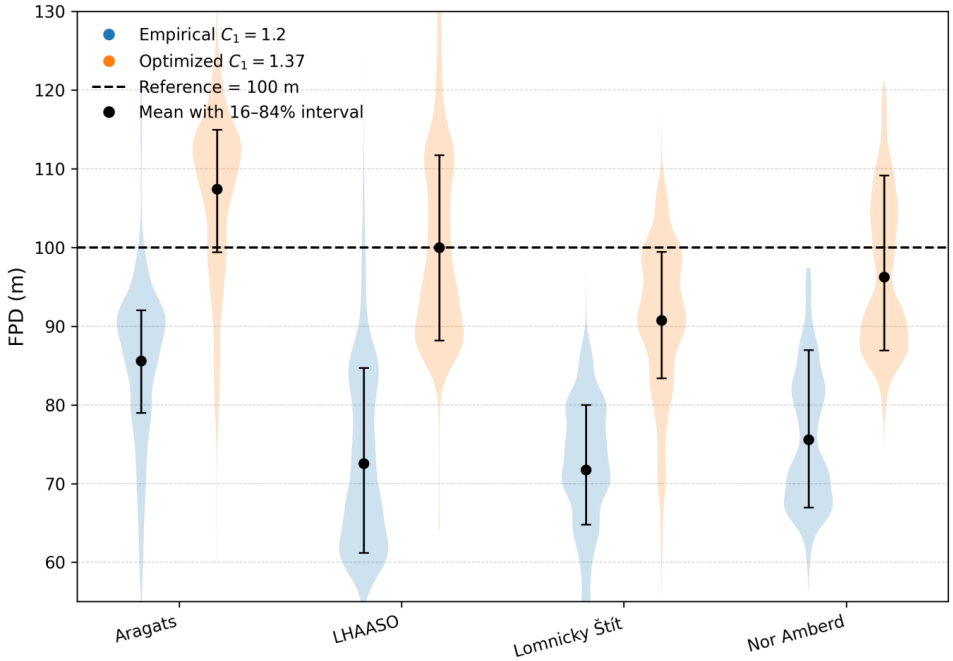

Figure 5.*Comparison of free path distance (FPD) distributions obtained using the empirical coefficient C_1 = 1.2 and the optimized value C_1 = 1.37 for four high-altitude stations (Aragats, LHAASO, Lomnický Štít, Nor Amberd). Distributions are derived from bootstrap resampling of the simulated spectra. Colored violins show the density of FPD values, while black markers denote mean values with 16th–84th percentile intervals. The dashed line indicates the reference propagation*

https://doi.org/10.5194/egusphere-2026-2078
Preprint. Discussion started: 20 May 2026

distance of 100 m between the electric-field boundary and the detector, highlighting the recovery of the correct physical scale with the optimized coefficient.

As shown in Fig. 5, the empirical coefficient $C_1 = 1.2$ systematically underestimates the FPD across all stations, whereas the optimized value $C_1 \approx 1.37$ restores the characteristic ~100 m propagation scale.

The optimized model consistently reproduces this distance for all stations, confirming the physical universality and robustness of the revised definition of C_1 across different atmospheric conditions.

The remaining deviations arise from statistical fluctuations of the high-energy spectral tails rather than limitations of the model.

5. Conclusions

In this work, we developed a unified physical framework for relativistic runaway electron avalanches (RREA) by combining the analysis of avalanche growth within the electric field with particle propagation beyond it. Using CORSIKA simulations at four high-altitude stations, all model parameters were derived directly from simulation data.

The results of this study reveal that the optimized coefficients derived from the CORSIKA simulations exhibit systematic differences between stations, indicating that the parameter K in Eq. (1) is not universal. The introduction of a density-dependent scaling term (Eq. (2)) resolves this discrepancy and yields a consistent description of avalanche growth across all considered altitudes. The negative exponent $a \approx -0.92$ reflects the fundamental role of atmospheric density in balancing electron acceleration and energy loss. In lower-density environments, reduced collision rates allow electrons to maintain higher energies over longer distances, resulting in larger avalanche lengths. Conversely, in denser air, increased interaction rates suppress avalanche growth.

Implementation of Eq.(2) with parameters $K = 6.39\times10^3$ kV and $a = -0.92$ provides a uniform estimation of the e-folding length across altitudes of 2000-6400 m. Applying the resulting equation to these heights will yield consistent, reliable estimates without requiring tuning for each altitude.

Investigation of the FPD empirical equation leads to justification of Eq. (3) with coefficients $C_1 \approx 1.37$, which remains stable across all considered altitudes. This result indicates that the internal energy structure of the avalanche is governed by intrinsic cascade dynamics and is largely independent of environmental conditions. In contrast, particle propagation beyond the electric-field region is controlled by density-dependent energy losses. The coefficient $C_2(h)$, derived from ESTAR stopping-power data, varies systematically with atmospheric density and determines the attenuation of electrons during transport.

https://doi.org/10.5194/egusphere-2026-2078
Preprint. Discussion started: 20 May 2026

These results demonstrate that RREA can be described as a two-stage physical system: avalanche growth inside the electric field, governed by density-dependent scaling, and particle transport outside the field, governed by density-dependent energy losses, linked by a universal energy-partition mechanism at the field boundary. The proposed formulation provides a compact, physically transparent description of both processes and establishes a consistent basis for interpreting high-energy particle phenomena in thunderstorm environments at different altitudes.

Code and data availability

All materials required to reproduce the results presented in this study that are under the author's control are publicly available at Zenodo:

https://doi.org/10.5281/zenodo.19508875 (Hovhannisyan, 2026)

An identical copy of the dataset is also available at Figshare:

https://doi.org/10.6084/m9.figshare.31980552

The Zenodo record should be considered the primary reference, while the Figshare repository is provided as an alternative access point.

The archived materials include all CORSIKA input files used in the simulations, definitions of the atmospheric electric-field configurations, auxiliary analysis scripts, processed simulation outputs, and all figures and tables presented in the manuscript, together with documentation describing the workflow required to reproduce the results.

The CORSIKA simulation framework is a licensed third-party Monte Carlo code developed and maintained by the Karlsruhe Institute of Technology (KIT). Due to licensing restrictions, the source code cannot be redistributed. The exact version used in this study (CORSIKA 7.7500) is specified in the manuscript and can be obtained for scientific use directly from the official distribution portal.

These materials enable reproduction of the analysis workflow and reported results for users with legitimate access to the CORSIKA framework.

Author contributions

L. Hovhannisyan designed the study, performed simulations, analyzed the data, and wrote the manuscript.

Competing interests

The author declares that there are no competing interests.

https://doi.org/10.5194/egusphere-2026-2078
Preprint. Discussion started: 20 May 2026

Acknowledgements

The author gratefully acknowledges Prof. A. Chilingarian for valuable discussions, guidance, and scientific support.

Financial support

This research received no external funding.

https://doi.org/10.5194/egusphere-2026-2078
Preprint. Discussion started: 20 May 2026

References

Bethe, H. A., and Heitler, W.: On the stopping of fast particles and on the creation of positive electrons, Proceedings of the Royal Society of London A, 146, 83–112, 1934, https://doi.org/10.1098/rspa.1934.0140.

Buitink, S., Corstanje, A., Falcke, H., et al.: Amplified radio emission from cosmic ray air showers in thunderstorms, Astronomy & Astrophysics, 503, 331–337, 2009, https://doi.org/10.1051/0004-6361/200911709.

Chilingarian, A., Hovsepyan, G., and Hovhannisyan, A.: Particle bursts from thunderclouds: Natural particle accelerators above our heads, Physical Review D, 82, 043009, 2010, https://doi.org/10.1103/PhysRevD.82.043009.

Chilingarian, A., Martirosyan, H., and Hovhannisyan, L.: Recovering of energy spectra of relativistic electrons and gamma rays measured during thunderstorm ground enhancements, Astroparticle Physics, 123, 102489, 2020, https://doi.org/10.1016/j.astropartphys.2020.102489.

Chilingarian, A., Khanikyants, Y., and Mailyan, B.: On the origin of high-energy radiation observed in thunderstorm ground enhancements, Atmosphere, 13, 2022, https://doi.org/10.3390/atmos13020250.

Dwyer, J. R.: A fundamental limit on electric fields in air, Geophysical Research Letters, 30(20), 2055, 2003, https://doi.org/10.1029/2003GL017781.

Dwyer, J. R., Smith, D. M., and Cummer, S. A.: High-energy atmospheric physics: Terrestrial gamma-ray flashes and related phenomena, Space Science Reviews, 173, 133–196, 2012, https://doi.org/10.1007/s11214-012-9894-0.

Dwyer, J. R., and Uman, M. A.: The physics of lightning, Physics Reports, 534, 147–241, 2014, https://doi.org/10.1016/j.physrep.2013.09.004.

Fishman, G. J., Bhat, P. N., Mallozzi, R., et al.: Discovery of intense gamma-ray flashes of atmospheric origin, Science, 264, 1313–1316, 1994, https://doi.org/10.1126/science.264.5163.1313.

Gurevich, A. V., Milikh, G. M., and Roussel-Dupré, R.: Runaway electron mechanism of air breakdown and preconditioning during a thunderstorm, Physics Letters A, 165, 463–468, 1992, https://doi.org/10.1016/0375-9601(92)90348-P.

Heck, D., Knapp, J., Capdevielle, J. N., Schatz, G., and Thouw, T.: CORSIKA: A Monte Carlo code to simulate extensive air showers, Report FZKA 6019, Forschungszentrum Karlsruhe, Karlsruhe, Germany, 1998.

https://doi.org/10.5194/egusphere-2026-2078
Preprint. Discussion started: 20 May 2026

503 Koch, H. W., and Motz, J. W.: Bremsstrahlung cross-section formulas and related data, Reviews of
504 Modern Physics, 31, 920–955, 1959, https://doi.org/10.1103/RevModPhys.31.920.

505 Sato, T.: Analytical model for estimating terrestrial cosmic ray fluxes nearly anytime and anywhere in
506 the world: Extension of PARMA/EXPACS, PLoS ONE, 11(12), e0160390, 2016,
507 https://doi.org/10.1371/journal.pone.0160390.

508 Hovhannisyan, L.: Data and code for "Relativistic runaway electron avalanches: unified
509 density-dependent scaling and transport", Zenodo, https://doi.org/10.5281/zenodo.19508875,
510 2026.